Proceedings of the 8th National Meeting of Synchrotron Radiation Users, Podlesice, September 24–26, 2009

Defect Structure Formed at Different Stages of Growth Process in Erbium, Calcium and Holmium Doped YVO_4 Crystals

A. Malinowska[a,*], E. Wierzbicka[a], M. Lefeld-Sosnowska[b], K. Wieteska[c], W. Wierzchowski[a], T. Łukasiewicz[a], M. Świrkowicz[a] and W. Graeff[d]

[a]Institute of Electronic Materials Technology, Wólczyńska 133, PL-01-919 Warsaw, Poland

[b]Institute of Experimental Physics, University of Warsaw, Hoża 69, PL-00-681 Warsaw, Poland

[c]Institute of Atomic Energy, PL-05-400 Otwock-Świerk, Poland

[d]HASYLAB at DESY, Notkestr. 85, D-22603 Hamburg, Germany

The defect structure of YVO_4 single crystals doped with Er^{3+}, Ho^{3+} and Ca^{2+} were studied by X-ray diffraction topographic methods, using laboratory and synchrotron radiation sources. Variously developed block structure was the dominating imperfection of the investigated crystals observed both in conventional Lang and synchrotron topographs. The evaluation of block misorientation was realised by means of superimposed projection and section white beam synchrotron radiation topographs. More possibilities of following the mutual rotation of blocks were provided by means of white beam synchrotron radiation WBSR projection topographs exposed through the fine mesh.

PACS numbers: 61.72.Ff

1. Introduction

Yttrium orthovanadate (YVO_4) is one of the most important laser host material providing high quantum efficiency and low excitation level when doped with rare-earth ions. It is especially useful in micro-laser systems, pumped with semiconductor laser diodes. In these applications the crystal should be highly doped with the rare-earth elements like Er^{3+} and Ho^{3+} and with Ca^{2+}.

YVO_4 crystallises in zircon-type tetragonal structure with space group $I4_1/amd$ and lattice parameters $a = b = 0.712$ nm and $c = 0.629$ nm [1]. The crystal structure enables efficient introduction of the required ions.

Some results, concerning the growth of YVO_4 and defects in these crystals are described in Refs. [1–8]. The main difficulty in the applications is obtaining of the crystals with low concentration of defects. Several defects, such as dislocations, low-angle grain boundaries, are usually generated even in the undoped material during crystal growth process [3, 8]. The defects can significantly decrease the efficiency of the laser elements. The formation of the defects is connected with the thermal strains occurring during both, the growth and cooling process. Other important technological problem is the tendency for the spiral growth of the crystal.

The aim of the paper is the investigation of growth defects in YVO_4 crystals doped with erbium, holmium and calcium in comparison to undoped YVO_4 crystals.

* corresponding author; e-mail: malinows@if.pw.edu.pl

2. Experiment

Single crystals of YVO_4 were grown in the nitrogen atmosphere by the Czochralski method with the use of Cyberstar Oxypuller 20-04 equipment. The thermal system consists of a 50 mm diameter and 50 mm high iridium crucible, and a passive afterheater of 60 mm diameter placed on the ceramics around the top part of the crucible. Inductive heating with the Huttinger generator was applied. To suppress the "tail" formation and to keep temperature gradient over the melt as stable as possible, the crucible was lifted up during growth runs to compensate melt level lowering. The charge material was prepared as a stoichiometric mixture of 4.5N purity oxides Y_2O_3, V_2O_5, Er_2O_3, Ho_2O_3, and CaO. All the dopants were substituted for yttrium. The distribution coefficient of erbium and holmium, determined with the use of inductively coupled plasma-optical emission spectroscopy (ICP-OES) were taken into account: $k_{Er} \approx 0.87 \pm 0.03$, $k_{Ho} \approx 0.91 \pm 0.03$. The following conditions of the growth process have been applied: growth rate 1–3 mm/h, rotation rate 15–30 rpm; cooling after growth — at least 24 h. As a result, good quality, [100]-oriented YVO_4 single crystals doped with Er (0.5 at.%) and Ca (0.4 at.%) or with Ho (5 at.%) were obtained. Their diameters and lengths were up to 25 mm and 50 mm, respectively.

The samples for X-ray topographic studies were cut out perpendicularly to the growth axis from different regions of the crystal — near the seed, in the middle, in the end part, and from the spiral growth part — in order to reveal possible changes of the defect structure during

the growth process. All samples were mechanically and chemically polished to the thickness of about 200 μm.

Characterisation of defect structure was performed by X-ray diffraction topographic methods. The conventional Lang projection X-ray topographs were taken in transmission and back-reflection geometry using Mo K_{α_1} radiation, for symmetric reflections and different sample azimuths. The topographs were recorded on 50 μm Ilford L4 nuclear plates.

The white beam synchrotron radiation (WBSR) back--reflection projection and section topographs were taken at low glancing angle of 5° at the Station F1 at HASYLAB (DESY, Hamburg). The section topographs were recorded using 5 μm slit. For studying of the subgrain structure the projection topographs were also taken through the metal fine mesh with 0.7 mm wire spacing, placed behind the crystal. That allows visualisation of the separate blocks misorientation by the displacement of the mesh wire shadows [9].

In all reproduced topographs dark tones correspond to high X-ray intensity.

3. Results

The X-ray diffraction topographic studies of YVO_4 crystals doped with ions Er^{3+} and Ca^{2+} were performed for samples cut out near the seed, in the middle and near the end of the crystal. In the case of YVO_4 crystal doped with Ho^{3+} ions the investigated samples were cut out only from the spiral growth part.

No segregation fringes were observed in the studied crystals, indicating good homogeneity of chemical composition. The most frequently observed crystal lattice imperfection were subgrain boundaries separating crystal blocks with slightly different orientation, as we can see in Figs. 1–5.

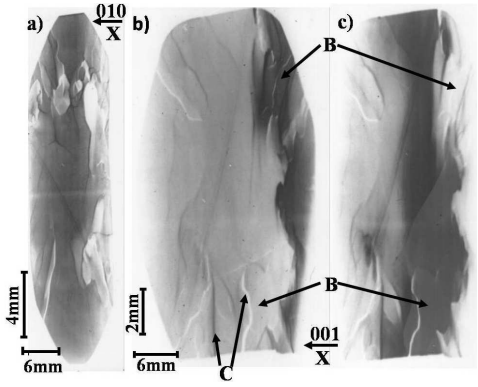

Fig. 1. X-ray back-reflection projection topographs of YVO_4 single crystal doped with 0.5 at.% Er; sample cut out near the seed; Mo K_{α_1} radiation, 800 reflection; (a) projection of incident beam direction on the film along [010]-direction; (b), (c) projection of incident beam direction on the film along [001]-direction, topographs taken for angular crystal setting differing through 0.1°; the difference in lattice orientation, being of the order of 0.1°, results in the opposite diffraction contrast of same regions (blocks) in both topographs (examples marked by B). X — projection of incident beam direction on the film. C — grain boundaries.

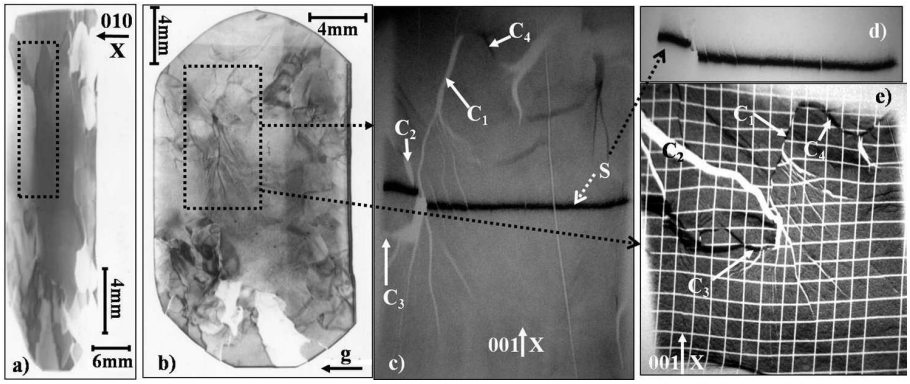

Fig. 2. Topographs of YVO_4 single crystal doped with 0.5 at.% Er; sample cut out from the middle part of the crystal: (a) X-ray back-reflection projection topograph, Mo K_{α_1} radiation, 800 reflection; (b) X-ray transmission projection topograph, Mo K_{α_1} radiation, 020 reflection, g — projection of the diffraction vector on the film; (c) WBSR projection topograph (of the selected region) with superimposed section topograph (marked by S); (d) WBSR section topograph (image of the slit, marked also by S in Fig. 2c); (e) WBSR back-reflection projection topograph (of the same region as in Fig. 2c) taken through the fine mesh with 0.7 mm wire spacing. X — projection of synchrotron radiation beam direction on the film. C — grain boundaries.

The Lang topographs obtained for samples YVO_4 doped with 0.5 at.% Er are shown in Figs. 1–3. In Fig. 1, representing a topograph for a sample cut out near the seed, one can notice regions, in which the intensity of the reflected X-ray beam are different one from another. They correspond to the crystal blocks of different incli-

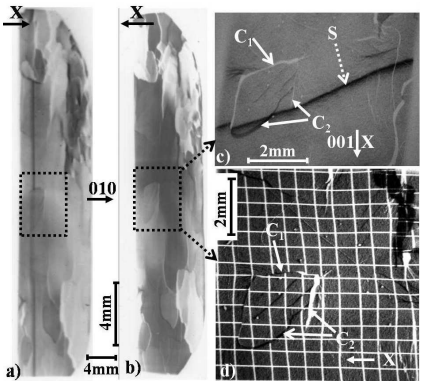

Fig. 3. Topographs of YVO_4 single crystal doped with 0.5 at.% Er; sample cut out near the end of the crystal; (a), (b) X-ray back-reflection projection topographs, Mo K_{α_1} radiation, 800 reflection; (c) WBSR projection topograph (of the selected region) with superimposed section topograph (image of the slit, marked by S); (d) WBSR back-reflection projection topograph (of the same region as in Fig. 3c) taken through the fine mesh with 0.7 mm wire spacing. X — projection of synchrotron radiation beam direction on the film. C — grain boundaries.

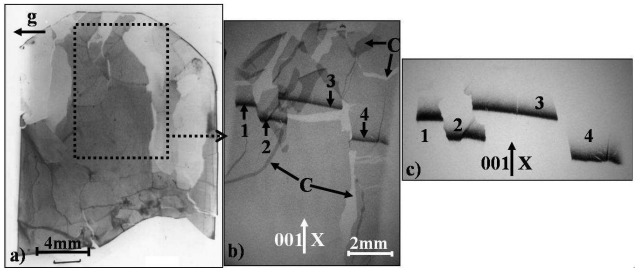

Fig. 4. Topographs of YVO_4 single crystal doped with 0.4 at.% Ca; sample cut out near the seed of the crystal; (a) X-ray transmission projection topograph, Mo K_{α_1} radiation, 020 reflection, g — projection of the diffraction vector on the film; (b) WBSR projection topograph (of the selected region) with superimposed section topograph (marked by S); (c) WBSR section topograph (image of the slit, marked also by S in Fig. 4b). X — projection of synchrotron radiation beam direction on the film. C — grain boundaries.

nation to the reflecting plane. The white or black lines represent grain boundaries (examples are marked by C). Figures 1b and c were taken for different angular crystal setting: (b) $\theta = 25.6°$, and (c) $\theta = 25.5°$. It is seen that blocks, giving black contrast in topograph in Fig. 1b, show opposite diffraction contrast to that of the same region in topograph in Fig. 1c (marked by B). This can be interpreted as a result of difference in lattice orientation, being of the order of 0.1°.

The topographs, obtained for the sample cut out in the middle of the crystal, are shown in Fig. 2. One can see some similarities between Fig. 2a and Fig. 1a. The transmission topograph in Fig. 2b reveals more details

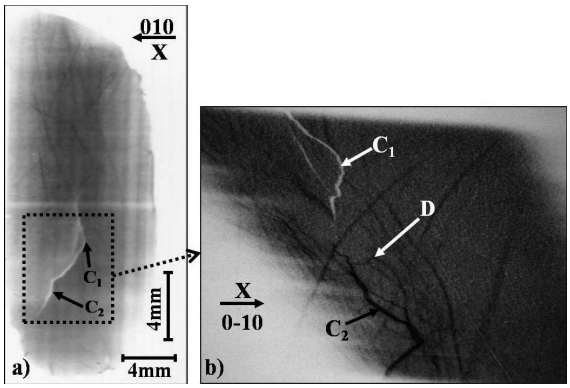

Fig. 5. Topographs of YVO_4 single crystal doped with 5 at.% Ho; sample cut out from the spiral part of the grown crystal; (a) X-ray back-reflection projection topograph, Mo K_{α_1} radiation, 800 reflection; (b) WBSR projection topograph (of the selected region). X — projection of synchrotron radiation beam direction on the film. C — grain boundaries.

projected from the whole sample thickness, whereas the back-reflection topograph in Fig. 2a reveals the image of the thin near-surface layer. We observe the similar configuration of crystal blocks in topographs obtained for the sample cut out near the crystal end (Figs. 3a, b) taken for two azimuths differing through 180°, where nearly complementary inversion of the contrast is seen. Topographs obtained for the sample cut out parallel to the crystal growth axis also reveal the crystal blocks and grain boundaries along the crystal growth direction.

Differently from the Lang topographs the WBSR topographs reveal the same diffracted beam intensity from all blocks but reflected along slightly different directions (Figs. 2c, d, 3c, d, 4b, and 5b). This is revealed through a mutual displacement of images of the blocks causing distinct white or black contrasts on their boundaries (examples are marked by C).

The WBSR topographs enable some evaluation of lattice misorientation between neighbouring blocks, which may be significantly improved by additional exposing of section topographs (Figs. 2d and 4c) or taking topographs through fine mesh (Figs. 2e and 3d). That may be followed in the superimposed projection and section topographs of the crystal fragment in Figs. 2c, 3c and 4b. Due to the lattice deformation the image of the slit is divided into a few mutually displaced segments, in some cases even slightly bent.

This different orientation may also be followed in the reproduced shadows of the mesh wires, seen in Figs. 2e and 3d. In particular case of undeformed crystal, all net elements are of the same rectangular or equilateral shape. The deformation of the mesh enables the evaluation of block misorientation similarly as the width of the contrast of the blocks boundaries. More information about the direction of the reflected beam can be obtained by following the shape of the particular net el-

ements (examples are marked by C in Figs. 2e and 3d). The misorientation between the blocks evaluated from the synchrotron topographs is of the same order of about several arc minutes.

In many cases the WBSR projection topographs, usually recorded at a large distance from the crystal — 10–15 cm, allow for better recognition of the boundaries between grains with small misorientation than in the case of some of the Lang topographs. Some dot-like tiny contrasts inside the block seen also in the synchrotron topographs may be interpreted as the dislocation outcrops.

The topographs of YVO_4 doped with Ca^{2+} show more developed block structure with greater number of smaller blocks and larger lattice misorientation (Fig. 4). In case of the YVO_4: Ho^{3+} crystal the samples cut out only from the spiral part of the grown crystal were investigated. The samples are more perfect than those cut out from the crystals doped with Er^{3+} and Ca^{2+}. In the topograph, obtained in back-reflection geometry (Fig. 5), the block structure is not well developed. Only one grain boundary was observed (marked by C). Some contrasts (marked by D), similar to those observed in undoped YVO_4 crystals [7], may probably be connected with dislocations.

4. Conclusions

- The YVO_4 single crystals doped with Er^{3+}, Ho^{3+} and Ca^{2+} were studied by X-ray diffraction topography methods, using laboratory and synchrotron radiation sources;
- The samples, cut out from different parts of the crystals — near the seed, in the middle, near the end and, in the case of YVO_4:Ho, from the spiral crystal growth region — were investigated;
- The dominating imperfection of the investigated crystals was variously developed block structure, which was observed in both conventional Lang and synchrotron topographs;
- The segregation fringes were not observed in any of studied crystals, indicating good homogeneity of chemical composition;
- The improved evaluation of block misorientation was realised by means of superimposed projection and section WBSR topographs. Even more possibilities of following the orientation changes including detection of mutual rotation of blocks were provided by WBSR projection topographs exposed through the fine mesh. The evaluated misorientation between various blocks was in the range of 5–40 arc minutes;
- The possible reason of the block formation during the growth process can be the thermal strains during cooling of the crystal;
- The present results did not reveal significant changes between the samples cut out from different regions of the crystals;
- The influence of doping was not very strong in the investigated crystals but the most developed grain structure was observed in the case of Ca-doped crystal and a little less distinct in the case of Ho-doped one. Comparing the results with the ones obtained for YVO_4 undoped crystals, presented by Wieteska et al. [8] we can see that block structure is more distinct in doped crystals than in undoped ones.

Acknowledgments

Synchrotron investigations were supported by the HASYLAB project II-20060165 EC. The technical assistance of J. Bondziul (Warsaw University) is highly appreciated.

References

[1] B.C. Chakoumakos, M.M. Abraham, L.A. Boatner, *J. Solid State Chem.* **109**, 197 (1994).

[2] S. Wu, G. Wang, J. Xie, X. Wu, G. Li, *J. Cryst. Growth* **249**, 176 (2003).

[3] D.E. Eakins, J.B. LeBret, M.G. Norton, D.F. Bahr, *J. Cryst. Growth* **266**, 411 (2004).

[4] S. Erdei, M. Klimkiewicz, F.W. Ainger, B. Keszei, J. Vandlik, A. Süveges, *Mater. Lett.* **24**, 301 (1995).

[5] S. Zhang, X. Wu, X. Yan, D. Ni, Y. Song, *J. Cryst. Growth* **247**, 428 (2003).

[6] M. Kruczek, E. Talik, H. Sakowska, W. Szyrski, Z. Ujma, D. Skrzypek, *J. Cryst. Growth* **275**, e1715 (2005).

[7] B.Q. Hu, Y.Z. Zhang, X. Wu, X.L. Chen, *J. Cryst. Growth* **226**, 511 (2001).

[8] K. Wieteska, W. Wierzchowski, E. Wierzbicka, A. Malinowska, M. Lefeld-Sosnowska, T. Łukasiewicz, W. Graeff, *Acta Phys. Pol. A* **114**, 455 (2008).

[9] A.R. Lang, A.P. Makepeace, *J. Phys. D, Appl. Phys.* **32**, A97 (1999).